Kinematic Model of Transient Shape-Induced Anisotropy in Dense Granular Flow

B. Nadler*
Department of Mechanical Engineering, University of Victoria, Victoria, BC V8W 2Y2 Canada

F. Guillard and I. Einav†
School of Civil Engineering, The University of Sydney, Sydney NSW 2006, Australia

(Received 8 July 2017; revised manuscript received 30 November 2017; published 11 May 2018)

Nonspherical particles are ubiquitous in nature and industry, yet previous theoretical models of granular media are mostly limited to systems of spherical particles. The problem is that in systems of nonspherical anisotropic particles, dynamic particle alignment critically affects their mechanical response. To study the tendency of such particles to align, we propose a simple kinematic model that relates the flow to the evolution of particle alignment with respect to each other. The validity of the proposed model is supported by comparison with particle-based simulations for various particle shapes ranging from elongated rice-like (prolate) to flattened lentil-like (oblate) particles. The model shows good agreement with the simulations for both steady-state and transient responses, and advances the development of comprehensive constitutive models for shape-anisotropic particles.

DOI: 10.1103/PhysRevLett.120.198003

Constitutive models in granular physics consider particle sizes, yet mostly not particle shapes. The significance of particle shapes in granular media was examined, both experimentally and numerically [1–8], but not through a simple and concise mathematical theory. However, all naturally occurring granular flows are composed of nonspherical particles; sand particles, rocks, or pebbles always present a certain degree of asphericity [6,9,10]. Also in industry most particles are nonspherical [11,12], in particular, in agriculture and food processing where crops have elongated or flattened shapes, or in pharmaceutics with pills and drug capsules. Understanding how particle shape affects granular flows is therefore fundamental for these fields. Particle shape is challenging to consider in general, as arbitrary shapes necessitate two-dimensional close surface representations [13–16]. Here, we consider the simplest extension from spherical particles, through a single parameter that captures any ellipsoidal shape. This extension introduces the additional concept of particle orientation which can be defined uniquely for such particles (Fig. 1). The static packing and flow of such particles have been studied previously [17–22]. It has been observed [20–23] that elongated particles tend to reach an average steady-state angle in simple shear that is misaligned with the streamlines. The origin of this preferred orientation remains unclear, but it is proposed that this is related to the asymmetry of the flow relative to the streamlines. This can be reasoned since in simple shear, the principal directions of the rate of deformation are aligned 45° to the streamlines, but associated with extension and contraction. It was observed that particles tend to reach a steady-state orientation where the larger particle dimension lies between the streamline and the positive principal direction [20,21,23], yet there is a need for a model capable of predicting this steady-state orientation. The proposed model will address this point by recognizing that while alignment with streamlines is expected, additional driving forces attract particles to align with the positive principal direction due to extension, and to divert from the negative principal direction due to contraction. These additional effects drive the average orientation from a complete alignment with streamlines toward the positive principal direction. The preferred steady-state orientation has strong dependency on the particle shape. In addition, the particle shape strongly affects the degree of particle alignment (ordering), which increases dramatically for more ellipsoidal particles, as the new model will also capture.

In this Letter, we develop a purely kinematic continuum model to predict the average particle orientation and ordering based on the velocity field and particle shape. This model is then compared with discrete element method (DEM) simulations, showing a very good agreement under both steady-state and transient flows. We focus on ellipsoidal particles, such as rice, lentil, and drug capsules,

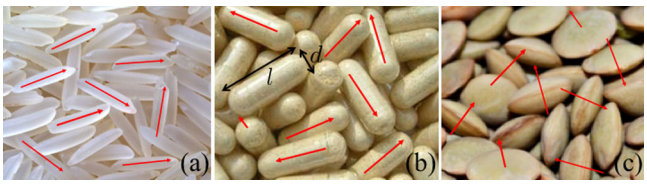

FIG. 1. Examples of oriented ellipsoidal particles. (a),(b) Rice and capsules ($r_g \equiv (l-d)/(l+d) > 0$), (c) lentils ($r_g < 0$).

 © 2018 American Physical Society

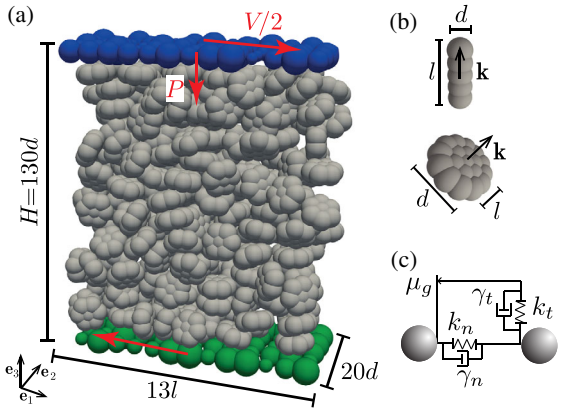

FIG. 2. (a) Typical geometry of the DEM simulations. (b) Dimension and orientation definition for elongated or flat particles used in simulation. (c) DEM contact model. Examples of video and snapshots from the simulations are given in the Supplemental Material [26].

where each particle is characterized by only two lengths d and l, with $d < l$ for prolate particles and $l < d$ for oblate particles [Fig. 2(b)]. The orientation of such particles can be defined unambiguously as the direction along the symmetry axis $\pm\mathbf{k}$. The statistical particle orientation at a given point in space and time can be represented by a probability density function f, such that $f(\mathbf{k}) \equiv f(-\mathbf{k}) \geq 0$ and $\oint_{S^2} f(\mathbf{k})da = 1$, where S^2 denotes the unit sphere. Simpler representations of the particle orientation distribution [24,25] can be obtained by using the Nth order tensorial moment of $f(\mathbf{k})$, where taking larger N gives a more refined representation of $f(\mathbf{k})$. Here we seek the simplest model using only the second order orientational tensor

$$\mathbf{A} = \oint_{S^2} f(\mathbf{k})\mathbf{k} \otimes \mathbf{k} da. \tag{1}$$

Using the symmetry property of $\mathbf{A}$, its spectral representation is $\mathbf{A} = \sum_{i=1}^{3} a_i \mathbf{a}_i \otimes \mathbf{a}_i$, where $1 \geq a_1 \geq a_2 \geq a_3 \geq 0$ are the eigenvalues, $a_1 + a_2 + a_3 = 1$, and $\{\mathbf{a}_1, \mathbf{a}_2, \mathbf{a}_3\}$ are the associated mutually orthogonal eigenvectors. The orientational tensor has two invariants. One can represent the degree of particle alignment, as an ordering measure defined by

$$\zeta = \sqrt{\frac{1}{2}((a_1 - a_2)^2 + (a_2 - a_3)^2 + (a_3 - a_1)^2)}, \tag{2}$$

where $0 \geq \zeta \geq 1$. The limit case of $\zeta = 0$ corresponds to isotropic distribution, while $\zeta = 1$ is when all particles are aligned along $\mathbf{a}_1$ and $a_1 = 1$, $a_2 = a_3 = 0$. A second meaningful invariant is defined and discussed in the Supplemental Material [26] as $\zeta_1 = (27/2)\det\{[\mathbf{A} - (1/3)\mathbf{I}]/\zeta\}$.

To develop a model for the evolution of the orientational tensor subjected to the velocity field $\mathbf{v}$, we first split the velocity gradient into its symmetrical part $\mathbf{D} = [\mathrm{grad}\,\mathbf{v} + (\mathrm{grad}\,\mathbf{v})^T]/2 = \mathbf{D}^T$, the rate of deformation, and antisymmetric part $\mathbf{W} = [\mathrm{grad}\,\mathbf{v} - (\mathrm{grad}\,\mathbf{v})^T]/2 = -\mathbf{W}^T$, the vorticity. We then propose the following two-parameters model for the orientational tensor:

$$\dot{\mathbf{A}} = \mathbf{WA} - \mathbf{AW} + \lambda[\mathbf{DA} + \mathbf{AD} - 2(\mathbf{A}\cdot\mathbf{D})\mathbf{A}] - \psi\|\mathbf{D}'\|(\mathbf{A} - \mathbf{I}/3) \tag{3}$$

where $\dot{\mathbf{A}}$ is the material time derivative of $\mathbf{A}$, $\mathbf{I}$ is the identity tensor, $\mathbf{A}\cdot\mathbf{D} = \mathrm{tr}\mathbf{A}\mathbf{D}^T$ is the scalar product, λ and ψ are model (constitutive) parameters, and $\mathbf{D}'$ is the deviatoric part of the rate of deformation. The evolution Eq. (3) is formulated by taking the time derivative of Eq. (1) $\dot{\mathbf{A}} = \oint_{S^2} f(\mathbf{k})(\dot{\mathbf{k}} \otimes \mathbf{k} + \mathbf{k} \otimes \dot{\mathbf{k}})da$, where $\mathbf{k}$ is a material line element and the area element da convects with the rotation of the particles, such that $f(\mathbf{k})da$ is constant in time. Since $\mathbf{k}$ is a material line element, $\dot{\mathbf{k}} = \mathbf{Wk} + \lambda\mathbf{Dk}$, where $\mathbf{W}$ and $\mathbf{D}$ are independent of $\mathbf{k}$ and can be taken outside of the integration. Finally, we add a correction term to satisfy the traceless requirement and a relaxation toward isotropic distribution. This evolution law satisfies the frame indifference (objectivity) requirement.

The material parameter λ governs the tendency to align with the rate of deformation, $\mathbf{D}$. It follows that $\lambda = 0$ for spherical particles and $\|\lambda\|$ increases as the particles become more ellipsoidal, with $\|\lambda\| \to 1$ as one of the particle dimension vanishes. In addition, λ is positive for prolate particles and negative for oblate particles since the larger dimension of the particle tends to align with the streamlines. Alternatively, for $\|\lambda\| = 1$ the particle orientation completely convects with the flow; hence, $\|\lambda\|$ can be seen as a measure of orientation attachment to the flow. Discrete contacts and collisions between particles also drive the particles to misalign. To include this we assumed that relaxation toward isotropic distribution is proportional to the granular temperature, usually seen proportional to the shear rate $\|\mathbf{D}'\|$. The relaxation parameter ψ must be nonnegative as relaxation is assumed to be toward isotropic distribution, and is anticipated to decrease for more ellipsoidal particles and hence reacts less to collisions. For further formulation it is convenient to define the shape ratio as $r_g \equiv (l - d)/(l + d)$. This shape measure takes the values $-1 < r_g < 1$, where r_g vanishes for spherical particles, is positive and increasing with the elongation for prolate particles, and negative and decreasing with the particle flatness for oblate particles. The model parameters can depend on all the objective characteristics of the system, e.g. particle shape, particle size, rate of deformation, the orientational tensor etc. However, for simplicity we limit our study to the simplest case where the model parameters are only functions of the shape ratio, that is

$\lambda(r_g)$ and $\psi(r_g)$. Furthermore, although there is no specific requirement for symmetry between prolate and oblate particles, for simplicity we take $\lambda(-r_g) \approx -\lambda(r_g)$ and $\psi(-r_g) \approx \psi(r_g)$.

To examine the performance of the kinematic model Eq. (3) and to determine its parameters, we carried out DEM simulations with LIGGGHTS [27] in a three dimensional simple shear configuration [Fig. 2(a)]. Two walls made of spheres having imposed motion separated by H and with normals $\pm\mathbf{e}_3$ apply: (1) shear motion with relative constant velocity $V = 0.5$ m.s^{-1} in the $\pm\mathbf{e}_1$ directions; and (2) constant pressure $P = 900$ Pa on the medium. The simulations are periodic in the $\pm\mathbf{e}_1$ and $\pm\mathbf{e}_2$ directions, and contain 1000–5000 shaped particles obtained by rigidly connecting spheres of diameter $d = 0.0015$ m and density $\rho = 2500$ kg m^3 together [Fig. 2(b)] leading to a typical inertial number of 6×10^{-3}. Although the obtained shaped particles are not strictly speaking ellipsoids, this method is chosen for its simplicity and efficiency. The interaction between individual spheres belonging to distinct shaped particles is dictated by a Hertz normal contact law with normal and tangential dissipation and friction [Fig. 2(c)] [28]. The normal force between the particles is modeled by a Hertzian spring with stiffness $k_n = 81 \times 10^3$ N m$^{-3/2}$ and viscous damping with viscosity $\gamma_n = 0.06$ kg s^{-1} m$^{-1/4}$; the tangential contact force is modeled similarly with a stiffness $k_t = 86 \times 10^3$ N m$^{-3/2}$ and viscosity $\gamma_t = \gamma_n$. The tangential force is limited by a Coulomb friction coefficient $\mu_g = 0.5$. The particles are displaced according to their contact forces by a Verlet algorithm. More details are available in the appendix of [29]. Neglecting any boundary effect, the flow is simply characterized by the shear rate $\dot{\gamma} = V/(2H)$, with

$$\mathbf{D} = \dot{\gamma}(\mathbf{e}_1 \otimes \mathbf{e}_3 + \mathbf{e}_3 \otimes \mathbf{e}_1),$$
$$\mathbf{W} = \dot{\gamma}(\mathbf{e}_1 \otimes \mathbf{e}_3 - \mathbf{e}_3 \otimes \mathbf{e}_1) \quad (4)$$

being the homogeneous rate of deformation and vorticity, respectively.

The discrete form of the orientational tensor $\mathbf{A}$ of an assembly of L particles is $\mathbf{A}_D = (1/L)\sum_{i=1}^{L} \mathbf{k}_i \otimes \mathbf{k}_i$. The model parameters are determined by comparing the orientational tensor in the steady-state of an ideal simple shear obtained by the model, $\mathbf{A}_M^S$, and the one computed from the DEM simulations, $\mathbf{A}_D^S$, such that $\min_{\lambda,\psi}\|\mathbf{A}_M^S - \mathbf{A}_D^S\|$, where $\|\|$ is the standard Euclidean norm. For a given value of r_g, the parameters λ and ψ can be determined such that the model and the DEM simulation show excellent agreement with $\|\mathbf{A}_M^S - \mathbf{A}_D^S\|/\|\mathbf{A}_D^S\| \approx 10^{-2}$. This suggests that the model well captures the salient physics of the particle orientation and alignment represented by the orientational tensor since only two parameters are used to predict the orientational tensor which consists of 5 degrees of freedom. We determine the parameters $\lambda(r_g)$ and $\psi(r_g)$, as shown in Figs. 3(a) and 3(b), using simple shear simulations with $-1 < r_g < 1$. Two empirical relationships satisfying the numerical measurements are then proposed: $\lambda(r_g) = (2/\pi)\tan^{-1}(5.5r_g)$ and $\psi(r_g) = 0.85\exp(-4r_g^2)$. These functions are merely curve fitting with no particular physical significance. The fits are based on data in the range $r_g \in [-0.6, -0.2]$ and $r_g \in [0.2, 0.7]$ and might not be accurate for small or large values of $\|r_g\|$. Furthermore, although we found rate independence in the low inertial number regime studied, it is likely that under much higher strain rates the functional forms of λ and ψ would further depend on the inertial number. The preferred orientation, $\mathbf{a}_1$, lies in the plane $\mathbf{e}_1 - \mathbf{e}_3$ as expected, and the misalignment angle from the streamlines (which are aligned with $\mathbf{e}_1$) is $\alpha = \tan^{-1}(\mathbf{a}_1 \cdot \mathbf{e}_3)/(\mathbf{a}_1 \cdot \mathbf{e}_1)$. It should be noted that α is different from the average angle of the distribution. In Figs. 3(c) and 3(d) the ordering, ζ, and the misalignment, α, are depicted as a function of r_g, showing good agreement between the model prediction and the orientation properties measured in simulations. It is interesting to note that for slightly nonspherical particles the misalignment angle converges to ≈20° from the streamlines, while the ordering vanishes.

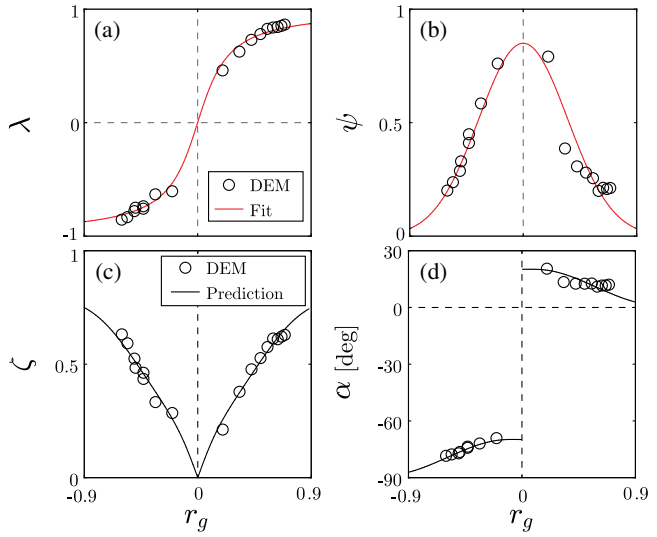

FIG. 3. (a), (b) Material parameters λ and ψ as a function of the shape ratio r_g. (c), (d) Model prediction for ordering, ζ, and misalignment angle, α, subjected to simple shear.

The ordering and orientation are completely described by the tensor quantity $\mathbf{A}$, which represents the second moment of the probability density function $f(\mathbf{k})$. However, the probability density function f cannot be accurately recovered from $\mathbf{A}$ alone. The optimal approximation is quadratic in $\mathbf{k}$, as shown in [30] and presented in Fig. 4. This approximation is exact for isotropic distribution $\mathbf{A} = (1/3)\mathbf{I}$ when $f(\mathbf{k}) = (4\pi)^{-1}$; however, the accuracy of this approximation diminishes as the alignment increases. For highly aligned particles this approximation

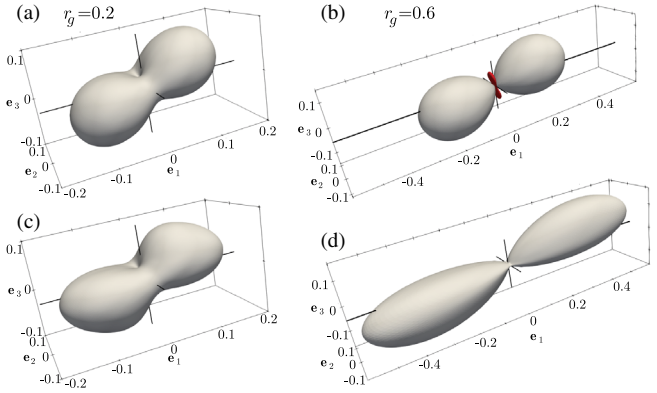

FIG. 4. Probability density function of particle orientation: (a), (b) based on optimal quadratic approximation in $\mathbf{k}$ given by [30] as $f(\mathbf{k}) \approx (15/8\pi)[\mathbf{k}\cdot(\mathbf{A}\mathbf{k}) - (1/5)]$, while (c), (d) measured from simulations. (a), (c) $r_g = 0.2$; (b), (d) $r_g = 0.6$. Red lobes in (b) are unphysical negative values.

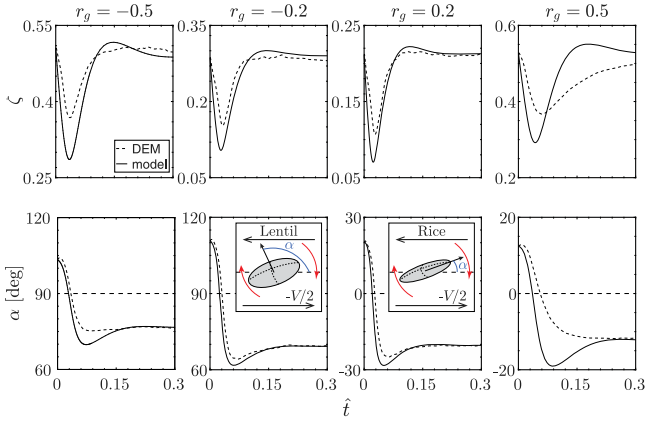

FIG. 5. Comparison of the model and DEM transient response over dimensionless time $\hat{t} = t|\dot{\gamma}|$ for various particle shapes. Insets: nontrivial tendency of particles to reorient after shear reversal.

can even predict negative values perpendicular to the major alignment axis which are unphysical. Figure 4 demonstrates that this approximation is acceptable for low ordering, $\zeta \approx 0.2$, but fails for high ordering $\zeta \approx 0.6$.

To further explore the performance of the kinematic model, the transient response is studied by a comparison with DEM numerical simulations. Initially, the numerical system is sheared in a particular direction until a steady state is obtained. The wall velocities are then reversed to the same shear rate in the opposite direction. This yields a transient response between two steady states which are a mirror reflection of each other. We also use the model to study the transient response and compare it with the numerical results, without changing λ and ψ, which were determined using the steady-state configurations. For the particular case of simple shear defined in Eq. (4), the direction reversal is obtained by changing the sign of the rate of shear $\dot{\gamma}$. It should be noted that while the steady state is very close to being homogeneous in the DEM simulations, hence justifying the homogeneous rate of deformation and vorticity as assumed in the model response, for the transient case this assumption is clearly incorrect as sharp reversal of the wall velocities imposes inertial propagation from the walls into the bulk which, at least initially, is not homogeneous [31]. Nevertheless, we use homogeneous strain rate and vorticity fields Eq. (4) to study the transient response of the model and for qualitative comparison with the DEM simulations. In addition, since constant pressure is imposed by the walls, the wall gap varies slightly during the transient response.

Figure 5 shows that the model well captures the trends of the transient responses observed in the simulations. Specifically, the transient response includes a significant reduction in the ordering, as the particles realign with the flow, followed by an increase in the ordering and returning to the same ordered steady state. This response is less significant in the simulations, which can be attributed to the differences between the DEM and the model related to the homogeneity of the velocity field. While the DEM transient is gradual as the transient propagates from the walls into the bulk, the model exhibits a homogeneous transient. The model shows overshooting of the ordering before returning to a steady state, while the simulations show insignificant or no overshooting. The orientation transient shows a somewhat unexpected response as the transients occur in the opposite direction of rotation to what is intuitively expected. Specifically, one might have expected the preferred orientation to rotate counterclockwise [with respect to Fig. 2(a)] during shear reversal to follow the new vorticity field. However, both the model and DEM show very similar response where the preferred orientation rotates in the clockwise direction opposite to the vorticity induced by the walls (Fig. 5 insets). As the transient propagates into the bulk yielding a more homogeneous field the overall rotation is clockwise, very similar to the prediction of the model. In addition, both the model and DEM show similar orientation overshooting before the steady state is obtained. It can be concluded that the model well captures qualitatively the transient response. The quantitative differences between the model and DEM could be attributed to the error introduced by the homogeneity approximation used in the model. This is supported by the observation that the model predicts a more profound and rapid transient than the DEM where the response is a gradual transient progressing from the walls into the bulk.

In summary, a kinematic model for the evolution of the alignment of ellipsoidal particles was proposed and compared with DEM simulations. The model consists of only two model parameters that for simplicity are assumed to depend only on the shape of the particles (shape ratio). In general, the material parameters should also depend on particle size, ordering, rates, etc.; however, this was not

considered here for simplicity. The two parameters were determined by comparison with DEM simulations of simple shear at a steady state. It was shown that the two parameters are sufficient to obtain a very good agreement of the full orientational tensor **A** between the model and the simulations. The transient response was used to further investigate the validity of the model. The model showed good agreement with the DEM simulations, capturing the essential transient features.

The stress response of an assembly of oriented particles has strong dependency on the alignment of the particles. While random distribution shows isotropic response, ordered arrangement shows increasing orthotropic properties with transverse isotropy as a special case. Hence, the stress response of an assembly of particles can vary from isotropic to increasing degree of orthotropy as the particle alignment (ordering) increases. The stress response of the oriented particles is outside the focus of this Letter; however, the representation of the particle alignment established in this Letter provides the foundation to further develop a stress response model of orthotropic elastic-viscoplastic material [32] that depends on the orientational tensor. Specifically, the principal directions of the orientational tensor, **A**, form the orthotropic basis, and the invariants govern the directional properties of the particle assembly. In addition, the current analysis was based on transient simple shear conditions, while other flow conditions would require further evaluation. Finally, beyond granular media and in the context of previous findings [33–36] the current treatment can also enrich the study of the reorientation of biological cells, magnetic particles, liquid crystals, and polymers.

*bnadler@uvic.ca
†itai.einav@sydney.edu.au

[1] J. C. Santamarina and G. C. Cho, in *Advances in Geotechnical Engineering: The Skempton Conference*, edited by R. J. Jardine, D. M. Potts, and K. G. Higgins (ICE Publishing, London, England, 2004), Vol. 1, p. 604.
[2] F. Alonso-Marroquin, S. Luding, H. J. Herrmann, and I. Vardoulakis, Phys. Rev. E **71**, 051304 (2005).
[3] A. Pena, R. Garcia-Rojo, and H. Herrmann, Granular Matter **9**, 279 (2007).
[4] T. Matsushima, J. Katagiri, K. Uesugi, A. Tsuchiyama, and T. Nakano, J. Aerosp. Eng. **22**, 15 (2009).
[5] J. Katagiri, T. Matsushima, and Y. Yamada, Granular Matter **12**, 491 (2010).
[6] T. Matsushima and C. S. Chang, Granular Matter **13**, 269 (2011).
[7] J. Tang and R. P. Behringer, Europhys. Lett. **114**, 34002 (2016).
[8] E. Azéma, I. Preechawuttipong, and F. Radjai, Phys. Rev. E **94**, 042901 (2016).
[9] H. Wadell, J. Geol. **40**, 443 (1932).
[10] J. K. Mitchell and K. Soga, *Fundamentals of Soil Behavior* (John Wiley & Sons, Hoboken, NJ, 2005).
[11] P. W. Cleary and M. L. Sawley, Appl. Math. Model. **26**, 89 (2002).
[12] C. González-Montellano, F. Ayuga, and J. Ooi, Granular Matter **13**, 149 (2011).
[13] E. T. Bowman, K. Soga, and T. W. Drummond, *Particle Shape Characterisation Using Fourier Analysis* (University of Cambridge, Cambridge, England, 2000).
[14] G. Mollon and J. Zhao, Granular Matter **15**, 95 (2013).
[15] D. A. H. Hanaor, Y. Gan, M. Revay, D. W. Airey, and I. Einav, Géotechnique **66**, 323 (2016).
[16] A. X. Jerves, R. Y. Kawamoto, and J. E. Andrade, Acta Geotechnica **11**, 493 (2016).
[17] M. Oda, S. Nemat-Nasser, and J. Konishi, Soils Foundations **25**, 85 (1985).
[18] G. W. Delaney and P. W. Cleary, Europhys. Lett. **89**, 34002 (2010).
[19] E. Azéma and F. Radjaı, Phys. Rev. E **81**, 051304 (2010).
[20] T. Börzsönyi, B. Szabó, G. Törös, S. Wegner, J. Török, E. Somfai, T. Bien, and R. Stannarius, Phys. Rev. Lett. **108**, 228302 (2012).
[21] T. Börzsönyi, E. Somfai, B. Szabó, S. Wegner, P. Mier, G. Rose, and R. Stannarius, New J. Phys. **18**, 093017 (2016).
[22] Y. Guo, C. Wassgren, W. Ketterhagen, B. Hancock, B. James, and J. Curtis, J. Fluid Mech. **713**, 1 (2012).
[23] F. Guillard, B. Marks, and I. Einav, Sci. Rep. **7**, 8155 (2017).
[24] S. G. Advani and C. L. Tucker, J. Rheol. **31**, 751 (1987).
[25] S. G. Advani and C. L. Tucker, J. Rheol. **34**, 367 (1990).
[26] See Supplemental Material at http://link.aps.org/supplemental/10.1103/PhysRevLett.120.198003 for simulation snapshots and video, and discussion on the second invariant ζ_1 of the orientational tensor **A**.
[27] C. Kloss, C. Goniva, A. Hager, S. Amberger, and S. Pirker, Prog. Comput. Fluid Dyn. **12**, 140 (2012).
[28] P. A. Cundall and O. D. Strack, Geotechnique **29**, 47 (1979).
[29] F. Guillard, Y. Forterre, and O. Pouliquen, Phys. Fluids **26**, 043301 (2014).
[30] K.-I. Kanatani, Int. J. Eng. Sci. **22**, 531 (1984).
[31] E. Rojas, M. Trulsson, B. Andreotti, E. Clément, and R. Soto, Europhys. Lett. **109**, 64002 (2015).
[32] M. B. Rubin and B. Nadler, Continuum Mech. Thermodyn. **28**, 515 (2016).
[33] A. Livne, E. Bouchbinder, and B. Geiger, Nat. Commun. **5**, 4938 (2014).
[34] G. B. Davies, T. Krüger, P. V. Coveney, J. Harting, and F. Bresme, Soft Matter **10**, 6742 (2014).
[35] C. Eringen, *Microrontinuum Field Theories II: Fluent Media* (Springer, New York, 1998).
[36] M. Kroger, *Models for Polymeric and Anisotropic Liquids* (Springer, New York, 2005).